U.S. Department of Commerce
National Oceanic and Atmospheric Administration
National Weather Service
National Centers for Environmental Prediction
5200 Auth Road
Camp Springs, MD 20746-4304

Office Note 452

COMPARISON OF STRATEGIES FOR THE SPECIFICATION OF ANISOTROPIES IN THE COVARIANCES OF A THREE-DIMENSIONAL ATMOSPHERIC DATA ASSIMILATION SYSTEM

Manuel S.F.V. De Pondeca*, R. James Purser, David F. Parrish, and John. C. Derber
Environmental Modeling Center, Camp Springs, Maryland
September 2006

.

*Email: Manuel.Pondeca@noaa.gov.

Abstract

Spatial recursive filters and the Hexad algorithm are used to implement four different models of anisotropic background error covariances within the NCEP Eta 3DVAR system. The covariance models are based on the Riishøjgaard method, the semigeostrophic and semigeostrophic-isentropic transformation methods, and the so-called kinematic deformation method. Each formulation uses background state diagnostics to define a distinct local aspect tensor of the assumed Gaussian correlation models. The forecast impacts of the various formulations are evaluated from simulations of a 2004 late winter storm over the continental U.S. All four covariance models used in the case study are found to have a significant, positive impact on the forecast skill measured in terms of the mean-squared errors of the 500 hPa geopotential height and the precipitation equitable threat scores.

1. Introduction

The assumed covariance model for the background errors is a crucial component of any three-dimensional variational (3DVar) scheme that assimilates data to initialize a weather prediction model (Daley 1991). Traditionally, the covariance model in an operational 3DVar scheme has been rather simple in its spatial structure, being horizontally isotropic and homogeneous for each of the separated scalar components into which the full dynamical fields are typically resolved. The balanced (quasi-geostrophic) component, having more energy in its modes and in the errors of these modes (as measured by an energy norm), naturally has covariance with the dominant amplitudes, while the errors of the unbalanced divergent and rotational components are normally considered to be of a lesser amplitude and significance. However, as we migrate to progressively finer scales in our forecast models and their assimilation systems, it becomes less excusable to ignore strong horizontal anisotropies and vertically tilted meteorological structures that typify fronts, rainbands, and quasi-linear features of organized convection. Directional dependencies in the errors of the background are intuitively expected to mirror the horizontal and vertical stretching of the mesoscale features themselves to some degree, so the assumption that simple horizontally isotropic and untilted covariances will suffice seems less easy to justify.

In this study, preliminary results of the impact of various covariance shapes on the analysis and forecast within the NCEP Eta 3DVar system are presented. The covariances possess a quasi-Gaussian form and are synthesized with the help of spatial recursive filters (Purser et al. 2003a). The sequential line-filtering Hexad algorithm (Purser et al. 2003b, Purser 2005), which is used with these filters, allows for the implementation of any arbitrary anisotropy, as prescribed by the centered and normalized second-moment aspect tensor of spatial dispersion, provided it is a sufficiently smooth function of space. Using the Riishøjgaard method (1998), the semigeostrophic and semigeostrophic-isentropic transformation methods (Desroziers, 1997), and the kinematic deformation method, the covariance shapes are prescribed as functionals of the background fields of Ertel potential vorticity, wind, and temperature under the assumption that the latent dynamical information these fields carry contains valuable information about the error correlations.

2. The Riishøjgaard Method

The current Gaussian horizontally isotropic model in use at NCEP can be expressed as:

$$C_o(\Delta\mathbf{x}) = \exp\left(-\frac{1}{2}\Delta\mathbf{x}^T\ \mathbf{S}_o^{-1}\Delta\mathbf{x}\right)\ , \qquad (1)$$

where $\Delta\boldsymbol{x}$ is the local three-dimensional Cartesian vector of separation between particle pairs. The inverse aspect tensor is the diagonal matrix:

$$\mathbf{S}_o^{-1} = diag\{L_h^{-2}, L_h^{-2}, L_v^{-2}\} \quad , \tag{2}$$

where L_h is the horizontal correlation length, L_v the vertical correlation length, and both may be considered functions of latitude and altitude.

Riishøjgaard (1998) suggests that a passively advected field would constitute a valuable indication of the recent flow distortions that have played a part in stretching the error covariances. For a chosen scalar function, q, assumed to be evolving predominantly under the influence of advection, the Riishøjgaard method preserves the assumed Gaussian model (1), while modifying the default aspect tensor (2) according to:

$$\mathbf{S}^{-1} = \mathbf{S}_o^{-1} + \frac{1}{L_q^2}(\nabla q)(\nabla q)^T. \tag{3}$$

L_q, which has the same units as q, represents a correlation scale in the "direction" of variations of q. Examples of a suitable choice for q might be the background humidity, potential temperature, or in order to respond more directly to dynamics, a standard form of potential vorticity (PV). For the case of Ertel PV, Fig.1 contours the covariance structure associated with a test point located near a region of strong PV gradient. As expected from the functional dependency expressed by (3), the contour lines of the covariance function tend to follow the isolines of the background PV.

3. Adaptation of the semigeostrophic transformation method of Desroziers

Following Desroziers (1997), we apply the following horizontal coordinate transformation of the semigeostrophic theory of Hoskins and Bretherton (1972), and Hoskins (1975):

$$x_g = x + \frac{1}{f}v_g \quad ; \quad y_g = y - \frac{1}{f}u_g \quad , \tag{4}$$

where f is the Coriolis parameter, (u_g,v_g) the geostrophic wind, and $\boldsymbol{x} = (x,y)$ and $\boldsymbol{x}_g = (x_g,y_g)$ are horizontal coordinates in real space and geostrophic-momentum space, respectively. Our computational approach, however, differs from that of Desroziers, who computes the complete set of coordinates in real space corresponding to the grid points of the transformed space. Instead, we opt for deriving the appropriate *2 x 2* aspect tensor of the real space, $\boldsymbol{S}$, that corresponds to the assumed spatially isotropic aspect tensor of the geostrophic-momentum space, $\boldsymbol{S}_g$. It is rather straightforward to show that under the assumed Gaussian covariance models these aspect tensors are related as:

$$\mathbf{S}^{-1} = \left(\frac{\partial \mathbf{x}_g}{\partial \mathbf{x}}\right)^T \mathbf{S}_g^{-1} \left(\frac{\partial \mathbf{x}_g}{\partial \mathbf{x}}\right) \quad , \tag{5}$$

where

$$\left(\frac{\partial \mathbf{x}_g}{\partial \mathbf{x}}\right) = \begin{bmatrix} 1 + \frac{1}{f}\frac{\partial v}{\partial x}, & \frac{1}{2f}\left(\frac{\partial v}{\partial y} - \frac{\partial u}{\partial x}\right) \\ \frac{1}{2f}\left(\frac{\partial v}{\partial y} - \frac{\partial u}{\partial x}\right), & 1 - \frac{1}{f}\frac{\partial u}{\partial y} \end{bmatrix}. \tag{6}$$

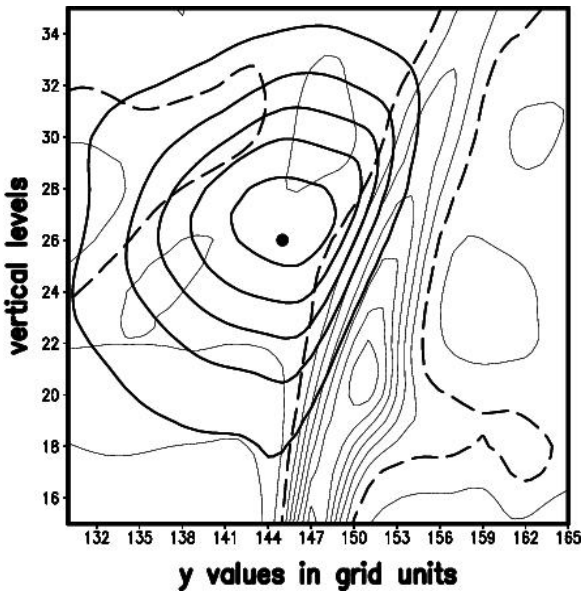

Fig.1: Riishøjgaard method: Dark contours represent the auto-correlation function for temperature on the y-z plane for a test point marked by the dot. Outermost contour value is 0.1 and contour interval is 0.2. Light contours represent background Ertel PV at 0.5 PVU contour interval (1PVU= 10^{-6} K kg^{-1} m^2 s^{-1}). Dark dashed contour marks the 1PVU line.

is the Jacobian matrix of the transformation. For simplicity, our calculations use the actual wind in place of the geostrophic wind, which explains why the subscript "*g*" was dropped from the wind components in (6). Since the vertical coordinate of the geostrophic-momentum space coincides with that of the real space, then for the full *3 x 3* aspect tensor: $(S^{-1})_{13} = (S^{-1})_{31} = (S^{-1})_{23} = (S^{-1})_{32} = 0$ and $(S^{-1})_{33} = L_v^{-2}$.

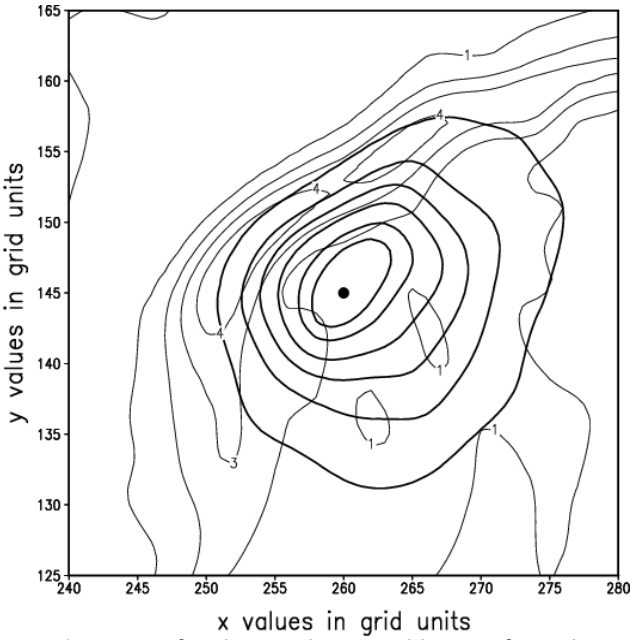

Fig.2: The same as in figure 1, except for the semigeostrophic transformation method, and light contours are now background absolute vorticity normalized by the Coriolis parameter.

Figure 2 illustrates the covariance shape for a test point in the vicinity of a strong gradient of background absolute vorticity due to the presence of an intense cyclone and accompanying cold front. It is apparent that unlike for the trivial case of the isotropic covariance shape, the isolines in this case tend to be stretched along the frontal boundary.

A natural generalization of the semigeostrophic equations to three dimensions is accomplished by using the isentropic surfaces (Hoskins and Draghici 1977) as the vertical transformed coordinate. Following Hoskins and Bretherton (1972), we define an effective physical height (actually a form of the Exner function of pressure):

$$z = \left(1 - \left(\frac{p}{p_o} \right)^{(R/c_p)} \right) z_o \quad , \tag{7}$$

where the constant z_0 is a vertical scale height and here $z_0 = 28000m$. The new Jacobian matrix generalizing (6) is

$$\left(\frac{\partial \mathbf{x}_{gi}}{\partial \mathbf{x}} \right) = \begin{bmatrix} 1 + \frac{1}{f}\frac{\partial v}{\partial x}, & \frac{1}{2f}\left(\frac{\partial v}{\partial y} - \frac{\partial u}{\partial x} \right), & \frac{1}{N_o}\frac{\partial v}{\partial z} \\ \frac{1}{2f}\left(\frac{\partial v}{\partial y} - \frac{\partial u}{\partial x} \right), & 1 - \frac{1}{f}\frac{\partial u}{\partial y}, & -\frac{1}{N_o}\frac{\partial u}{\partial z} \\ \frac{1}{N_o}\frac{\partial v}{\partial z}, & -\frac{1}{N_o}\frac{\partial u}{\partial z}, & \frac{N^2}{N_o^2} \end{bmatrix}, \tag{8}$$

in which the quantity N with $N^2 = (g/\theta)\partial\theta/\partial z$ approximates the Brunt-Väisälä frequency, and N_o is a reference standard value of N, which may be a function of height. The subscript *"i"* in $\boldsymbol{x}_{gi}$ stands for "isentropic."

4. Covariance based on kinematic deformation at finite time lag

In this construction, the assumption is that the actual covariance is the result of kinematic deformation over a finite time acting upon a passively evolving covariance that was initially horizontally isotropic and homogenous. For reasons of practicality, we make some additional simplifying assumptions. For example, the present local instantaneous deformation, $\boldsymbol{F} = (\partial \boldsymbol{v}/\partial \boldsymbol{x})$, where $\boldsymbol{v}$ is the velocity field, is assumed to be constant on the material parcel for the entire duration, T. For convenience, we evaluate the deformation $\boldsymbol{F}$ from the velocity field at the actual time. The effect of $\boldsymbol{F}$ in evolving an infinitesimal material displacement, $\Delta\boldsymbol{x}$, is described by the integrable equation,

$$\frac{d\Delta\mathbf{x}}{dt} = \mathbf{F}\,\Delta\mathbf{x} \ . \tag{9}$$

The cumulative effect upon a displacement that at time $t = 0$ is at $\Delta\boldsymbol{x}(0)$, is:

$$\Delta\mathbf{x}(t) = \mathbf{A}(t)\,\Delta\mathbf{x}(0)\,, \tag{10}$$

where

$$\mathbf{A}(t) = \exp\{t\mathbf{F}\} \quad . \tag{11}$$

Assuming Gaussian models of covariance and taking (10) into consideration, the following relationship can be derived between the actual aspect tensor $\mathbf{S}$ and the undeformed standard horizontally isotropic aspect tensor $\mathbf{S}_{-\mathbf{T}}$ at time $t = -T$:

$$\mathbf{S} = \mathbf{A}^{-1}(-T)\ \mathbf{S}_{-T}\,\mathbf{A}^{-T}(-T) \quad . \qquad (12)$$

Based on the same synoptic situation and test point as in Fig.2, Fig.3 shows the covariance of the kinematic deformation method for $T = 6h$. One sees that just as in Fig.2, the resulting covariance is confined to one side of the frontal system. Its shape, however, differs from that of Fig.2.

5. Results

5.1 Synoptic situation and methodology

The synoptic situation features a storm system with an associated cold front that moved from the Southwest United States into New Mexico and Texas on 4 March 2004. By 5 March 2004, a well developed cyclone was positioned over Eastern Iowa. Heavy rainfall and damaging winds were associated with the passage of this system as it progressed eastward through the Midwest and into the Appalachians.

The initial time in our case study is 12Z on 5 March 2004, from which a 12-hour assimilation cycle is run followed by a 72-hour free forecast. All computations are performed using the NCEP Eta 3DVar and forecast model. The horizontal resolution of the system is 12km with 60 vertical levels. The 12 hour assimilation cycle is broken into four pieces: a 3DVar analysis with a subsequent 3 hour forecast which, in turn, provides the background fields for the next analysis. The assimilation cycle and free forecast are run for each of the covariance models discussed above. The control run consists of a system using the horizontal, isotropic covariance model of equations (1) and (2).

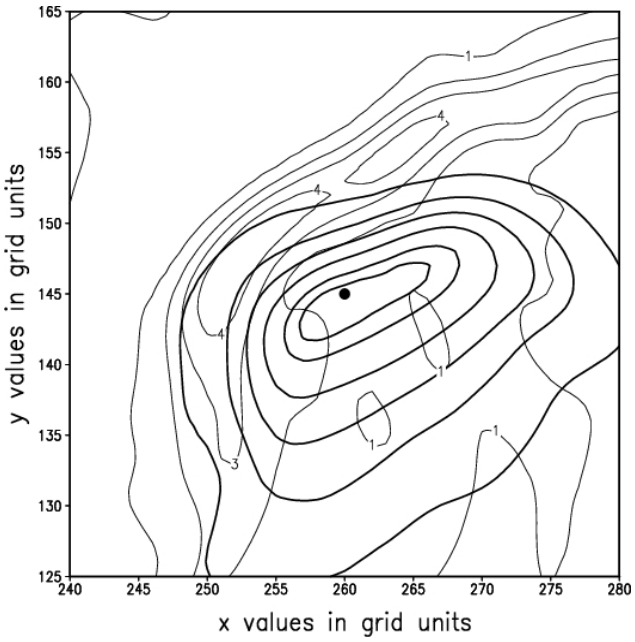

Fig.3: Same as in figure 2, except the auto-correlation function is calculated via the kinematic deformation method with T=6h.

Our forecast verification is based on the mean-squared errors for the 500 hPa geopotential height and the 24h accumulated rainfall. For each free forecast, we compute a skill score relative to the control forecast, which is defined as follows:

$$SS(t) = 1 - \frac{MSE(t)}{MSE_{control}(t)} \quad . \qquad (13)$$

$MSE(t)$ and $MSE_{control}(t)$ are the mean-squared errors of the 500 hPa geopotentail height for the experimental and the control forecast, respectively, and are evaluated with respect to the operational analysis (see Wilks, 1995). Here, "t" denotes the forecast time. Positive (negative) values of the SS indicate improved (degraded) forecasts with respect to the control, which is characterized by $SS(t) = 0$. The upper bound for this forecast measure is $SS(t) = 1$, which corresponds to a perfect forecast, while the lower bound is theoretically (-∞). In addition, we compute the equitable threat scores (ETS) and bias scores (BIA) for the 24-hour accumulated rainfall ending 12Z 6 March 2004. For a given rainfall threshold, these scores are computed as (eg. Hamill 1999):

$$ETS = \frac{a - a_\tau}{a + b + c - a_\tau} \qquad (14)$$

and

$$BIA = \frac{(a+b)}{a+c} \quad , \qquad (15)$$

with

$$a_\tau = \frac{(a+b)(a+c)}{a+b+c+d} \quad . \qquad (16)$$

In these expressions, a is the number of hits, b the number of false alarms, c the number of misses, d the number of correct negatives, ie., the number of locations with both forecast and verification rainfall below threshold, and a_τ is the expected number of hits in a random forecast.

5.2 Forecast skill scores of the 500 hPa geopotential height

Fig.4 shows the SS for the Riishøjgaard method, whereby the covariances are modeled to follow the background Ertel PV to some degree. The value of the function correlation length is $L_q = 2.10^{-6} K\ kg^{-1}m^2s^{-1}$ for both experiments reported in the figure. However, one of the experiments uses the original correlation lengths of the horizontally isotropic model of equations 1 and 2, while the other uses the correlation lengths of the isotropic model inflated by a factor of 50%. It should be noted that the effect of the second term in equation (3) is a contraction of the effective spatial correlation lengths, which thus justifies the compensating inflation. The results show positive SS for forecast times greater than 12 hours for both experiments, and the best results are found for the experiment that uses inflated correlation lengths.

Fig.5 shows the SS for the pure semigeostrophic transformation method, i.e., when the vertical coordinate z remains unchanged. The three distinct lines are for simulations that use (i) the original spatial correlation lengths of the horizontally isotropic model, (ii) the spatial correlation lengths of the horizontally isotropic model inflated by 15%, and (iii) the spatial correlation lengths of the horizontally isotropic model contracted by 15%. Except for the small positive SS values seen in two of the experiments one day into the forecast, Fig.5 reveals an overall forecast degradation.

The forecast SS for two experiments based on the semigeostrophic-isentropic transformation method are illustrated in Fig.6. The two lines correspond to two different ranges allowed for the ratio N^2/N_o^2 of the Jacobian matrix (8). The results for both experiments show positive SS values for most of the three-day forecast period. These results, in light of the largely negative results from the pure semigeostrophic

transformation method, suggest the importance of correctly specifying the vertical structure in the covariance model.

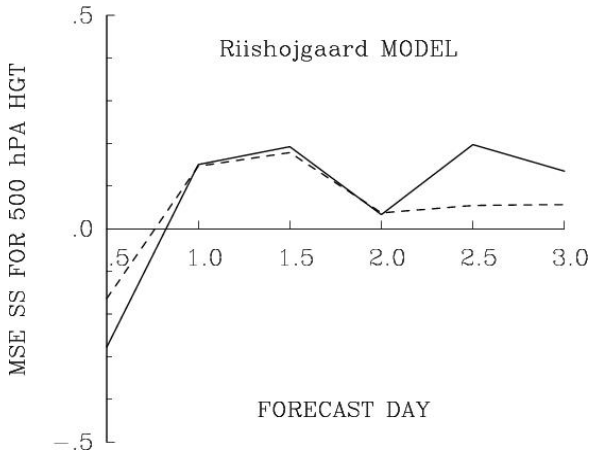

Fig.4: 500hPa geopotential height forecast skill scores for the Riishøjgaard method. Dashed line for experiment that uses the original correlation lengths of the isotropic model and continuous line for experiment that uses the correlation lengths of the isotropic model inflated by 50%.

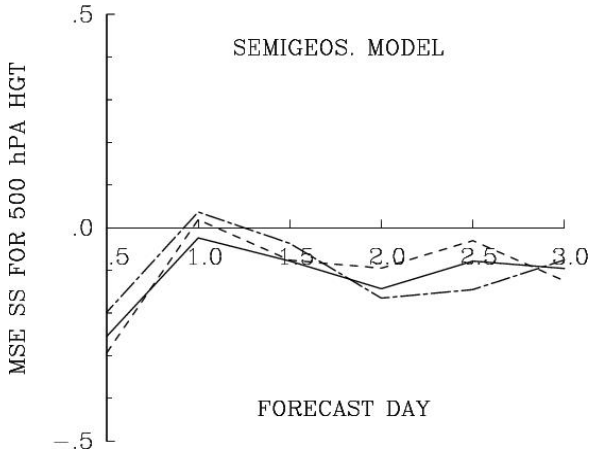

Fig.5: 500hPa geopotential height forecast skill scores for the semigeostropic transformation method. Continuous lines for experiment that uses the original correlation lengths of the isotropic model, dashed (dot-dashed) line for experiment with the correlation lengths of the isotropic model inflated (contracted) by 15%.

Fig. 7 displays the skill scores of three kinematic experiments that use different time lags, T=3, 6, and 12h, respectively. All three experiments yield positive SS for forecast times greater than one day. The SS for the experiment with T=6h, however, drop to negative values by day 3. The best results are obtained for T=12h. This figure clearly shows that the forecast SS in the kinematic method are sensitive to the specified time lag.

For all four methods, qualitatively similar results are obtained for the 300 hPa and 850 hPa geopotential height skill scores (not shown).

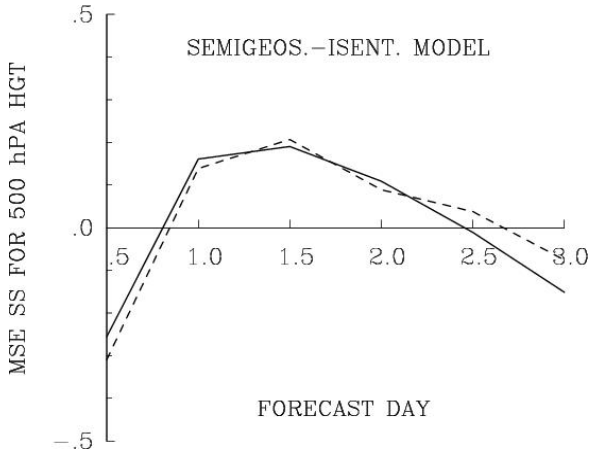

Fig.6: 500hPa geopotential height forecast skill scores for the semigeostrophic-isentropic transformation method. Continuous line for experiment with $0.75 \le N^2 \big/ N_o^2 \le 1.25$ and dashed line for experiment with $0.5 \le N^2 \big/ N_o^2 \le 2.0$. The horizontal correlation lengths are those of the original isotropic model of equations (1) and (2).

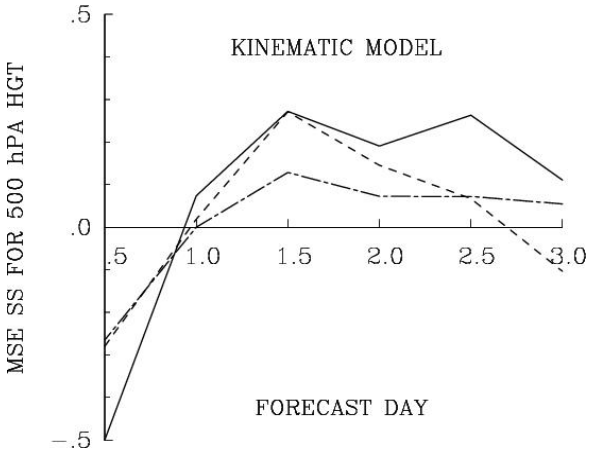

Fig.7: 500hPa geopotential height forecast skill scores for the kinematic method for T=12h (continuous line), T=6h (dashed line) and T=3h (dot-dashed line).

5.3 Accumulated Rainfall

For the analysis and the control run, figures 8 and 9 show the 24-hour accumulated rainfall ending 12Z 6 March 2004. The shortcomings of the control forecast are apparent from the intensity and location of the rainfall maxima that it produces.

Equitable threat scores and bias scores were computed for the 10 experiments of Figures 4 – 7. For each covariance method, figure 10 shows the ETS and BIA for the experiment that yields the best ETS. These are, namely, experiment with contracted spatial correlations lengths for the semigeostrophic method, experiment with $0.5 \le N^2 \big/ N_o^2 \le 2.0$ for the semigeostrophic-isentropic method, experiment with inflated spatial correlation lengths for the Riishøjgaard method, and experiment with T=6h for the kinematic deformation method.

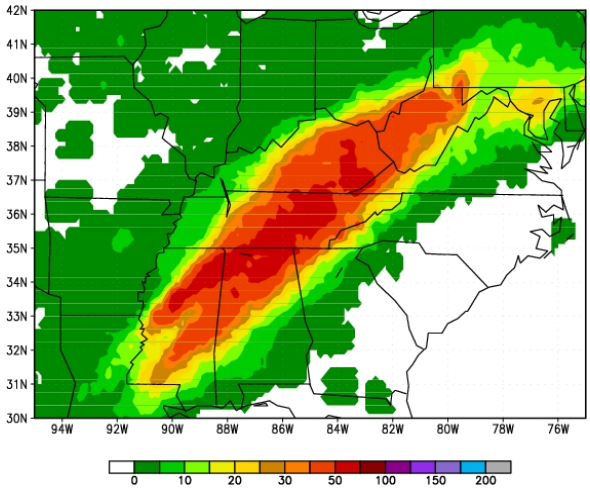

Fig.8: The observed 24h accumulated rainfall in mm ending 12Z 06 March 2004.

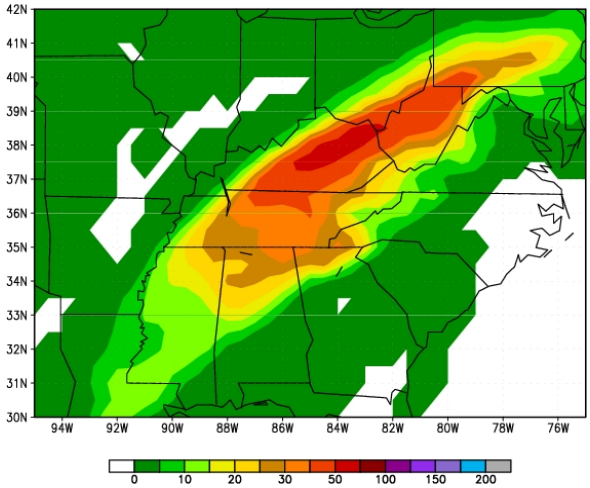

Fig.9: The 24h accumulated rainfall in mm ending 12Z 06 March 2004 and evaluated from the control run.

The results shown here are for the geographical region of figures 8 and 9. Qualitatively similar results were obtained for a larger domain covering the continental U.S. The ETS scores show that the experiments based on the Riishøjgaard method and the semigeostrophic transformation method yield the best rainfall improvements over the control forecast. The Riishøjgaard method leads to forecast improvements for rainfall thresholds between 1.27 mm and 50.80 mm, while the semigesotrophic experiment improves the forecast for thresholds above 10.16 mm, and degrades it for thresholds below this value. The experiments based on the semigesotrophic-isentropic transformation method and the kinematic method yield improved forecasts for thresholds above 27.94mm and mostly degraded forecasts for thresholds below this value. The bias scores show that the Riishøjgaard and kinematic experiments tend to underestimate the amount of rainfall for all thresholds, and that this is more pronounced for the kinematic case. In contrast, the direction of the bias for the experiments based on the semigeostrophic and semigeotrophic–isentropic methods depends on the threshold. It is also important to mention that, especially for the Riishøjgaard, semigeostrophic and

semigesotrophic-isentropic experiments, both the ETS and BIA were found to show little sensitivity to the parameter settings explored in this study for each covariance model (not shown).

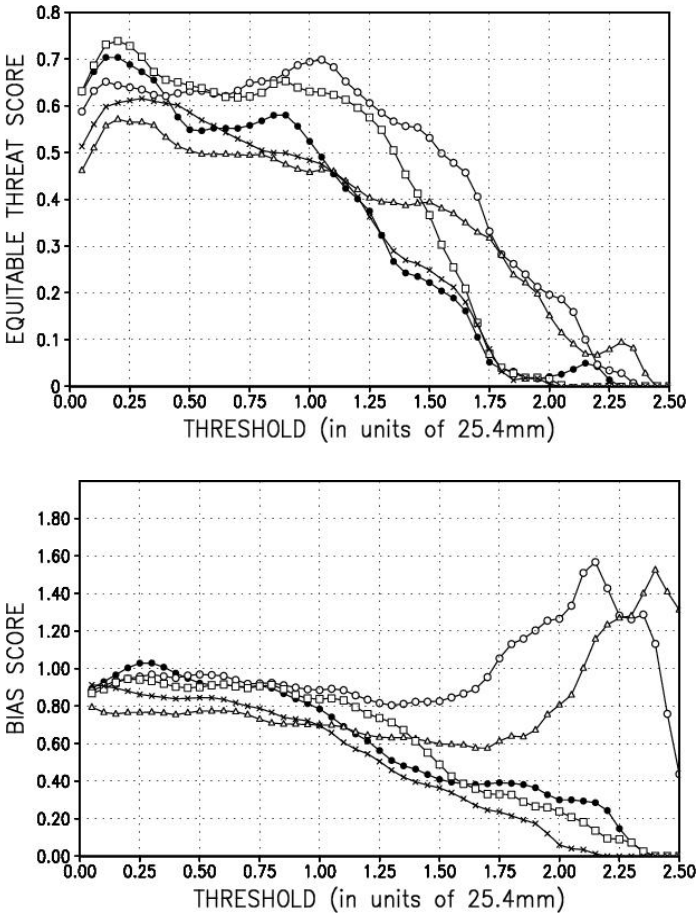

Fig.10: Equitable threat scores (upper panel) and bias scores (lower panel) of 24h-accumulated rainfall ending 12Z 06 March 2004 for the best experiment from each covariance model as measured by the best ETS. Line with closed circles for control forecast, line with open circles for semi-geostrophic method, line with open triangles for semigeostrophic-isentropic method, line with open squares for Riishøjgaard method, and line with multiplication signs for kinematic method.

Figures 11-14 display the 24 hour accumulated rainfall for the four experiments of Fig.10. Noticeable improvements in the intensity and overall location of the regions of heavy rainfall in the rainband are seen when the Riishøjgaard or the semigeostrophic methods are used. In particular, both experiments lead to increased rainfall over Tennessee and therefore to a better match with the observed pattern of Fig.8. It should be noted that the control experiment misplaces the regions of heavy rainfall further northeast, in Kentucky. An undesirable feature in the Riishøjgaard experiment of Fig.11 is the bend in the rainband south of Kentucky, into Tennessee, which is not verified by the observations. A slight improvement in the location of the rainfall maxima is also observed with the use of the semigeostrophic-isentropic and kinematic methods (see figures 13 and 14). It is interesting to mention that, out of the three kinematic experiments, the experiment with T=12h was found to produce a remarkable improvement in the location of the rainfall maxima (not shown). Its ETS scores, however, are in general lower than those corresponding to T=6h, which are shown in Fig.10.

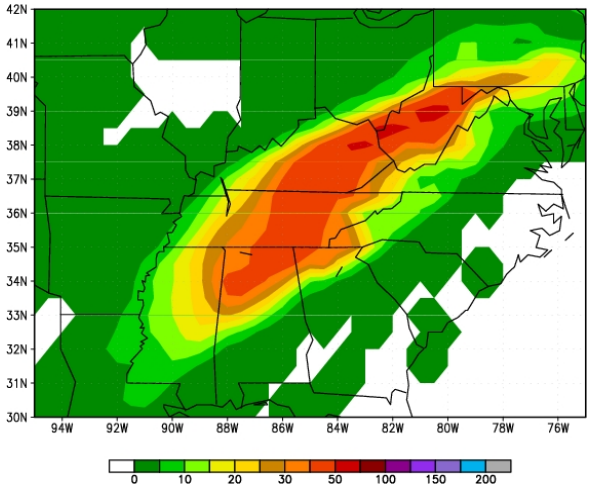

Fig.11: The best 24h accumulated rainfall in mm ending 12Z 06 March 2004 evaluated from the experiments that use the Riishøjgaard method. The best results correspond to the experiment that uses the spatial correlation lengths of the isotropic model inflated by 50%.

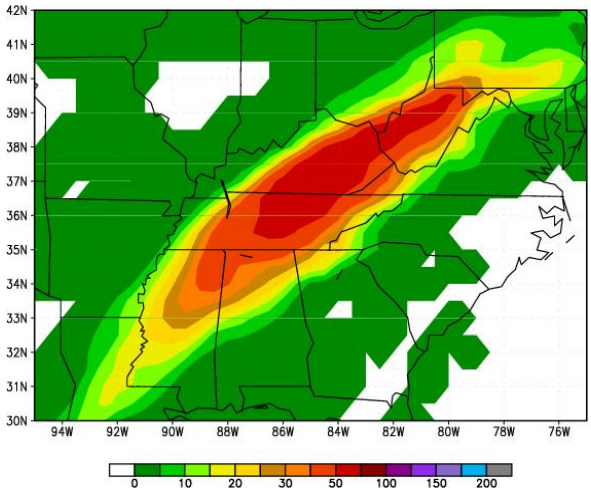

Fig.12: The best 24h accumulated rainfall in mm ending 12Z 06 March 2004 evaluated from one of the experiments that uses the semigeostrophic transformation method. The best results correspond to the experiment that uses the spatial correlation lengths of the isotropic model contracted by 15%.

Summary

Spatial recursive filters and the Hexad algorithm were used to implement four different anisotropic models of background error covariances within the Eta 3DVar system, and results were presented from a case study featuring a 2004 late winter storm. The covariance models based on the Riishøjgaard method, the semigeostrophic-isentropic method and the kinematic method were found to have a significant positive impact on the model forecast as measured by the 500 hPa geopotential height skill scores. In contrast, the covariance model based on the pure semigeostrophic transformation method was found to degrade the 500 hPa geopotential height for all parameter settings explored in this study. In addition, the skill scores for the Riishøjgaard and kinematic methods were found to display significant sensitivity to the parameter settings of the covariance model. Compared with the control forecast, noticeable improvements of the 24h accumulated rainfall were obtained with the use of the covariance models based on the Riishøjgaard method and the semigeostrophic method. In light of the poor 500 hPa geopotential height skill scores for the semigeostrophic

model, this result seems to suggest that the evaluation of the performance of a given covariance model might be in general metric dependent. Small, positive impacts on the 24-hour accumulated rainfall were also found with the use of the semigesotrophic-isentropic and kinematic covariance models. Furthermore, the equitable threat scores and bias scores for the 24-hour accumulated rainfall were found to display little sensitivity to the parameter settings when the Riishøjgaard, semigeostrophic, or semigeostrophic-isentropic methods were used.

Through a mixture of physical intuition and trial and error, these experiments provided an initial attempt at addressing the issue of how to choose the covariance models that are most appropriate to the mesoscale 3DVar systems. The results seem to suggest that all four models presented in this paper hold promise, and

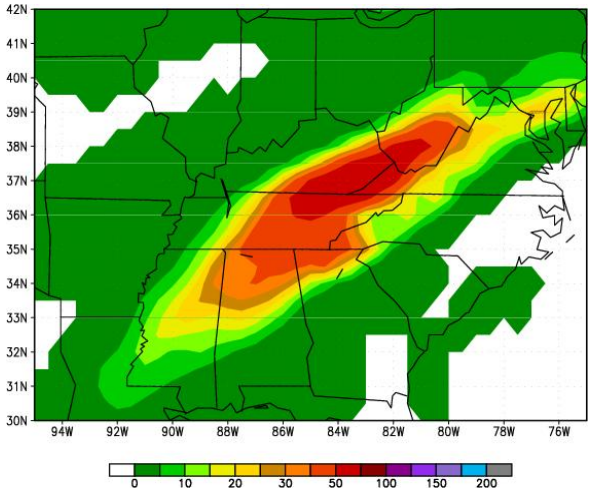

Fig.13: The best 24h accumulated rainfall ending 12z 06 March 2004 evaluated from the experiments that use the "semigeostrophic-isentropic method." . The best results correspond to the experiment with $0.5 \le N^2 / N_o^2 \le 2.0$.

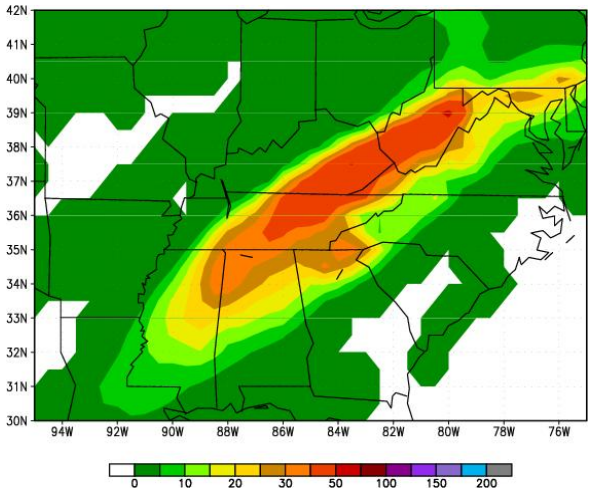

Fig.14: The best 24h accumulated rainfall ending 12Z 06 March 2004 evaluated from the experiments based on the kinematic method. The best results correspond to the experiment with T=6h.

that the parameter space associated with each model should be extensively explored before firm conclusions on the merits of each covariance model can be drawn. Various simulations for different synoptic situations and seasons must be considered, so that some statistical value can be associated with the results. We hope that the adaptive prescription of background error covariances will allow us to attain some of the benefits of 4DVar while retaining the lower computational costs of a 3DVar system. Finally, it is worthwhile to mention our recent realization that the methods presented in this paper can all be cast within the framework of a "generalized" Riishøjgaard method by appropriate simultaneous selection of a number of scalar fields $\{q_i\}$. This will be the subject of a future paper.

References

Daley, R. A. 1991: *Atmospheric Data Assimilation*. Cambridge University Press, 457 pp.

Desroziers, G. 1997: A coordinate change for data assimilation in spherical geometry of frontal structure. *Mon. Wea. Rev.*, **125**, 3030-3038.

Hamill, T. M., 1999: Hypothesis tests for evaluating numerical precipitation forecasts. *Wea. Forecasting.,* **14**, 155-167.

Hoskins, B. J., and F. P. Bretherton, 1972: Atmospheric frontogenesis models: mathematical foundation and solution. *J. Atmos. Sci.*, **29**, 11-37.

Hoskins, B. J., and I. Draghici, 1977: The forcing of ageostrophic motion according to the semigeostrophic equations and in an isentropic coordinate model. *J. Atmos. Sci.*, **34**, 1859-1867.

Hoskins, B. J., 1975: The geostrophic momentum approximation and the semigeostrophic equations. *J. Atmos. Sci.*, **32**, 233-242.

Purser. R.J., 2005: A geometrical approach to the synthesis of smooth anisotropic covariance operators for data assimilation. NOAA/NCEP Office Note 447, 60pp.

Purser, R. J., W.-S. Wu, D. F. Parrish, and N. M. Roberts, 2003a: Numerical aspects of the application of recursive filters to variational statistical analysis. Part I: Spatially homogeneous and isotropic Gaussian covariances. *Mon. Wea. Rev.*, **131**, 1524-1535.

Purser, R. J., W.-S. Wu, D. F. Parrish, and N. M. Roberts, 2003b: Numerical aspects of the application of recursive filters to variational statistical analysis. Part II: Spatially inhomogeneous and anisotropic general covariances. *Mon. Wea. Rev.*, **131**, 1536-1548.

Riishøjgaard, L. P., 1998: A direct way of specifying flow-dependent background error correlations for meteorological analysis systems. *Tellus,* **50A**, 42-57.

Wilks, D. W., 1995: Statistical Methods in the Atmospheric Sciences. Academic Press, San Diego, California, 467pp.